Nanotechnology **19** (2008) 145305 (7pp) doi:10.1088/0957-4484/19/14/145305

Surface enhanced Raman scattering on long-range ordered noble-metal nanocrescent arrays

Kebin Li, Liviu Clime, Bo Cui and Teodor Veres

NRC, Industrial Materials Institute, 75 Boul. de Mortagne, Boucherville, J4B 6Y4, Canada

Received 26 December 2007, in final form 28 January 2008
Published 4 March 2008
Online at stacks.iop.org/Nano/19/145305

Abstract

Long-range ordered noble-metal nanocrescent arrays of different sizes and shapes have been successfully fabricated by using both nanoimprint lithography and e-beam lithography techniques. Large surface enhanced Raman scattering (SERS) enhancements in the detection of rhodamine 6G (R6G) molecules on these arrays have been observed and attributed to the enhancement of the local electromagnetic (EM) fields near individual nanocrescents. Electromagnetic enhancement factors for crescents of different shapes are computed using the discrete dipole approximation and compared with experimental measurements of the R6G Raman intensities. It is found that the maximum values of SERS intensity appear at an intermediate value of the crescent eccentricity and the observed behaviour is related to the spatial distributions of the enhancement of the local EM field (hot spots).

(Some figures in this article are in colour only in the electronic version)

1. Introduction

Since its discovery in the 1970s [1, 2], surface enhanced Raman scattering (SERS) has been proven to be a sensitive technique in single molecule detection [3, 4]. Moreover, due to its chemical specificity and label-free nature, it attracts increasing attention in analytical, biomedical, environmental, as well as global and homeland security applications [5]. The giant enhancement of the Raman scattering is usually attributed to two well-known mechanisms, namely, the electromagnetic mechanism and charge transfer mechanism [6–10]. While the latter originates from the charge transfer interaction between adsorbates and metals, the former results from huge amplifications (enhancements) of the local electromagnetic (EM) field near roughened metal surfaces due to the excitation of intrinsic surface plasmonic resonances (SPR) of individual nanostructures as well as plasmonic coupling effects between adjacent nanostructures [11]. In order to explore and use the huge local field enhancement for practical applications, it is desirable to tune the SPR frequencies to match them with a given laser wavelength available. Therefore the design and fabrication of nanostructured SERS substrates in order to generate large local EM field in a controllable way at the narrow gap between nanostructures ('hot spots') becomes essential. For example, one can achieve enhancement factors of 10^{14} in aggregated colloids of metallic (silver or gold) nanoparticles [3, 12]. However, the limited stability and reproducibility of metal colloids often limit their practical application. Alternatively, various types of nanostructures have been suggested for enhancing the local EM field, such as sharp metal tips [13–15], dielectric conical tips coated with metal films [16–19], nanoparticles [20] and plasmonic lenses [21], sharp metallic grooves and nanowedges [22–25], nanoburgers [26], triangular nanoprisms [27], nanopins [12], nanocages and nanocubes [28, 29], nanobars and nanorice [30], as well as the recently reported nanocrescents (NC) [31–34]. Unlike the usual way of generating hot spots in the gap between two closed nanostructures, the NC array present hot spots located near individual NCs which do not originate in any mutual electromagnetic interaction and thus we call 'integrated hot spots'.

The NCs reported so far are fabricated by using a technique based on angle deposition of noble metals on spherical nanoparticles. Thus obtained nanostructures can be SERS active but lack long-range order and consequently limit their technological applications. In this work, we report on the fabrication of periodic arrays of noble-metal nanocrescents by both e-beam lithography (EBL) and nanoimprint lithography

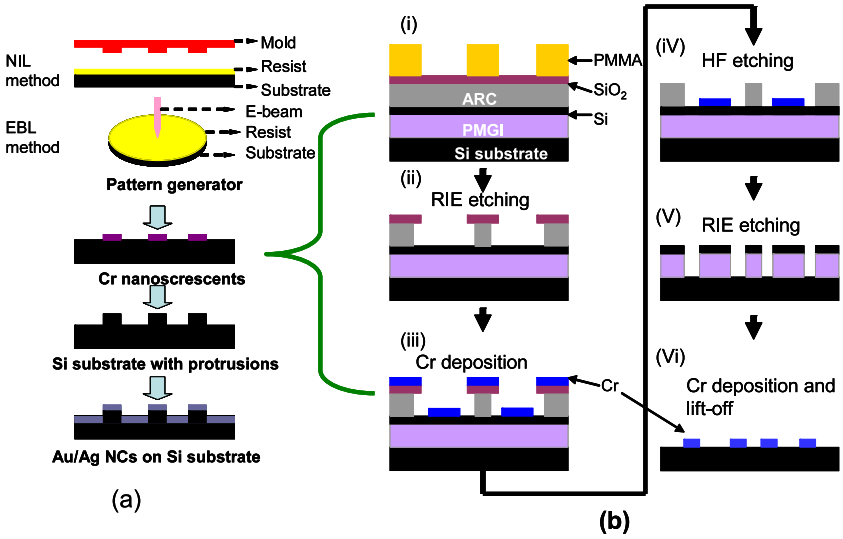

Figure 1. (a) Procedure of fabrication of the periodic arrays of Au/Ag nanocrescents by using NIL and EBL. (b) Process flow chart for fabrication of Cr nanocrescents by using NIL.

(NIL) techniques. SERS enhancements in the detection of R6G molecules have been systematically studied on these long-range ordered noble-metal NC arrays of different sizes and shapes. Additionally, based on a detailed numerical analysis of the local EM field enhancement by using the discrete dipole approximation (DDA) approach we analyse the distribution of the hot spots for different polarizations of the incident light and different geometries of the NCs. Both experimental and modelling results show that the SERS intensity can be optimized by adjusting the geometry of the NCs, the maximum SERS intensity appearing at an intermediate value of the crescent eccentricity. The observed behaviour is related to the intensity and the spatial distributions of the generated integrated hot spots near the NCs.

2. Experimental details

The procedure employed in order to fabricate long-range ordered arrays of noble-metal NCs consists of several steps, as schematically depicted in figure 1(a). The pattern of NCs is generated by using either NIL or EBL on Si substrates coated with either NIL resist or EBL resist. After chromium deposition by evaporation at normal incidence and then lift-off, Cr nanostructures in the shape of NCs are formed. The obtained Cr nanostructures are used as metal masks in reactive ion etching (RIE) (Oxford Instruments PlasmaLab 80 Plus) to transfer the pattern onto Si substrate. The etching depth is about 140 nm. The chromium leftovers after RIE etching are removed by using a commercial Cr etchant CR-4S (Cyanthek Corporation). This results in the Si substrate with Si nanoprotrusion with crescent-like profiled nanostructures. Gold and silver NCs are finally formed after deposition of the corresponding noble metals by evaporation at normal incidence on the pre-nanostructured Si substrate. The advantage of this approach over other fabrication methods for creating SERS active nanostructures on flat silicon substrate is obvious. The background Raman signal from the Si substrate at the high wavenumbers will be suppressed dramatically with the base area covered by the same metal. By controlling the deposition process of the noble-metallic thin film, we can minimize its contribution to the Raman signal of the patterned nanostructures thus putting more emphasis on the SERS performance and optimization of individual NC[1].

The process of the fabrication of Cr nanocrescents by using NIL is very similar to what has been published before [35]. The substrate used for NC fabrication by NIL process consists of five layers: (1) a layer of 160 nm PMGI (MICRO-CHEM) on Si; (2) 6 nm of evaporated Si; (3) a cross-linked anti-reflection coating (ARC) polymer layer (Brewer Science XHRiC-16) with a thickness of 200 nm; (4) 15 nm of evaporated SiO_2 and (5) 200 nm of PMMA (MICRO-CHEM) as NIL resist. The critical processing steps are schematically depicted in figure 1(b) and summarized as follows:

(i) an array of nanoholes with diameter of 60 nm and period of 200 nm were created by NIL on 4 inch Si wafer;
(ii) nanoholes are transferred to the 200 nm thick ARC layer and stopped at the 6 nm thick Si layer by reactive ion etching (RIE) with undercut;
(iii) deposition of 5 nm thick Cr layer by using e-beam evaporator to form a Cr nanodisc on the 6 nm thick Si layer;
(iv) use diluted HF solution (HF:water = 1:50) to lift-off the 15 nm thick SiO_2 layer together with the 5 nm Cr layer on top;
(v) use RIE to etch through the 6 nm thick Si layer by SF_6 gas at 10 mTorr and 100 W followed by O_2 plasma etching to form the NC shaped pattern in the 160 nm thick PMGI layer;
(vi) finally 15 nm thick Cr layer is deposited by using e-beam evaporator at normal incidence angle and lifted off, resulting in an array of Cr NCs on the Si substrate.

[1] In real applications, one can deposit noble metal in particle form, which can make an additional contribution to the SERS signal.

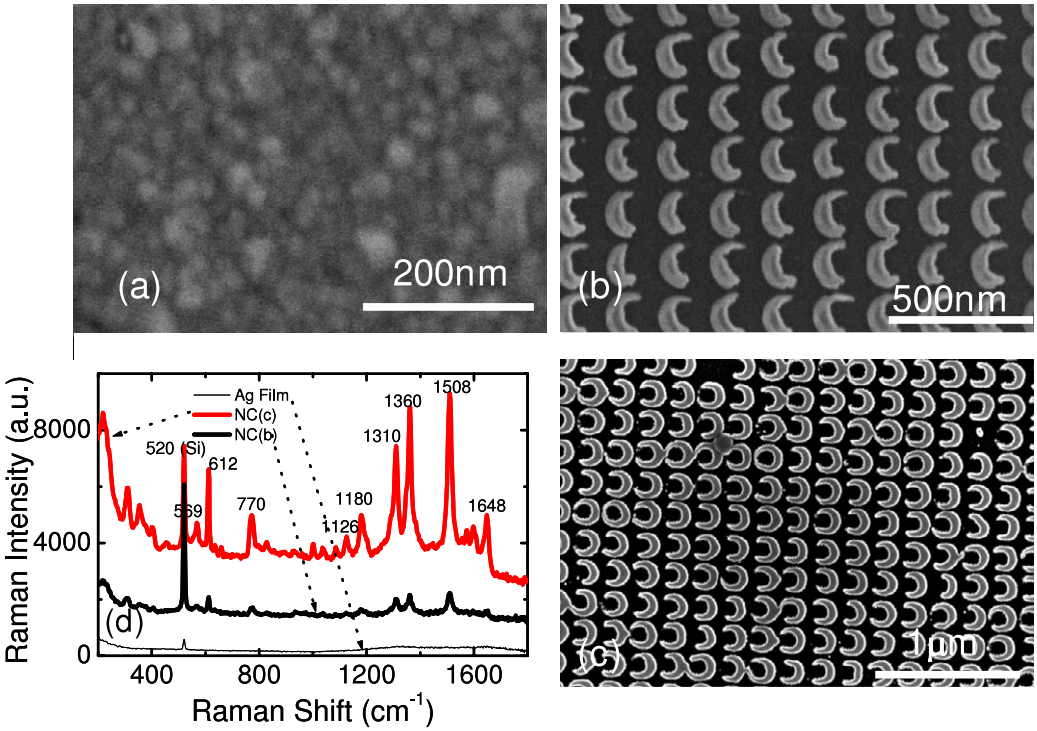

Figure 2. (a) SEM image of the continuous Ag thin film; (b) SEM image of Ag nanocrescents with large openings between two tips; (c) SEM image of Ag nanocrescent with small openings between two tips; (d) Raman spectra of R6G molecules coated at the concentration of 1×10^{-6} M on three different substrates whose SEM images are shown in (a)–(c).

In the NIL method, the width of the nanocrescent is controlled by the etching time of the first ARC layer while their size and period can be controlled by the imprinting mould and the NIL process.

The patterning of the periodic array of Cr nanocrescents can also be generated by EBL with the following process steps:

(1) A Si wafer is coated with about 70–90 nm thick PMMA layer,
(2) nanocrescents patterning with different diameters, openings and periods are created by using the Hitachi S4800 operated at 30 keV with a writing current of 30 pA and an exposure dose of 400 μC cm^{-2};
(3) after the development in a solution of the mixture of methyl isobutyl ketone (MIBK) (Sigma-Aldrich) with isopropyl alcohol (IPA) (MIBK:IPA = 1:3) for 15 s, 15 nm thick Cr thin film was deposited on the wafer by using e-beam evaporator at the deposition rate of 0.8 A s^{-1};
(4) in a last step, metallic Cr nanocrescents are formed after lift-off in acetone for 2 min under ultrasonic agitation.

The main advantage of the NIL over the EBL is obvious as it allows for fabricating large areas of long-range ordered nanostructures that can be duplicated rapidly. Moreover, the edges of the NCs obtained by NIL are much sharper than those obtained by EBL, which is in favour of generating larger local electromagnetic fields, thus increasing the SERS enhancement factor.

Rhodamine 6G (R6G, from Sigma-Aldrich) with a concentration of 1×10^{-3} M was obtained by dissolving 47.5 mg R6G powder into 100 ml deionized (DI) water. Aqueous R6G solutions with other concentrations are then obtained by further dilutions of this initial solution in DI water. The nanostructured substrates were functionalized with R6G by dipping them into an aqueous solution for about 1 h. Then the substrates were dried by using nitrogen blow. Raman spectra were acquired with a Raman Station R3 from Avalon Instruments operating at 785 nm. A thermoelectrically cooled charge coupled device (CCD) operating at −80 °C was used as detector with 2 cm^{-1} resolution. All spectra were collected at a fixed time of 3 s and calibrated with respect to the Raman peak of the silicon wafer at 520 cm^{-1}. The spot size of the laser and the maximum laser power intensity for 40× objective lens are about 25 μm and 0.15 mW μm^{-2}, respectively.

3. Results and discussion

Figures 2(b) and (c) are two typical SEM images of the Ag nanocrescents with height of 20 nm fabricated by NIL method. By controlling the fabrication process, we are able to create arrays of NCs with different tips but with a fixed period at 200 nm. The shape of a given crescent is specified by three parameters: R—the radius of the external (circumscribed) circle, r—the radius of the inner circle and the NC breadth d measured along the line going through the centres of these two circles (the symmetry axis of the NC). The ratio of d over $2R$ determines finally the opening of a NC. As shown in figures 2(b) and (c), here, $2R$ and d is about 160 and 50 nm, respectively. However the opening of the tips is larger in figure 2(b) than that in (c). For comparison, a SEM image of

the continuous Ag thin film taken on an area without NCs is shown in figure 2(a).

Figure 2(d) shows the Raman spectra taken on three samples with different surface structures and the corresponding SEM images are shown in figures 2(a)–(c). For the unpatterned area (the continuous Ag thin film), no apparent Raman peak of R6G is visible except that at 520 cm^{-1} which is attributed to the Raman peak of Si substrate. For the Ag NC with large openings shown in figure 2(b), the Raman peaks corresponding to R6G are obvious. An increase in the intensity of these peaks of R6G is enhanced for about six times when the opening of the NC becomes small as shown in figure 2(c). This shows that the NC alone can generate integrated hot spots with SERS enhancement factors depending on the geometry of the crescent.

In order to understand the distribution of the hot spots in the NC, SPR spectra and near-field local EM field distribution of noble-metal NCs were calculated using a multiprocessor implementation of DDA [36–38] method and a lattice dispersion relation (LDR) prescription [37] for individual polarizabilities at the nodes of the mesh. Theoretical comparative studies with Mie theory [39] or experimental measurements of absorption spectra of nanowires [40] and energy-loss spectroscopy (EELS) visualizations of near fields on nanostructures [41] demonstrated the accuracy of DDA in computing both internal and scattered fields. In our model, the NCs are meshed with a resolution of about 3 nm, small enough to achieve high accuracy from the DDA algorithm [36]. Absorption efficiencies and near-field enhancements were thus computed for gold and silver NCs with fixed external curvature radius but different breadths and thicknesses. The Raman intensity was evaluated by using the parameter

$$I \propto \int\int_S \left(\frac{E}{E_0}\right)^4 \mathrm{d}S \tag{1}$$

where E is the electric field magnitude, E_0 is the EM field of the incident light beam and S the irradiated surface area of the NC. Since accurate evaluations of the Raman intensities need additional knowledge about Raman tensors of probe molecules, their adsorption configuration as well as coupling effects of these molecules with the local EM field [42], the parameter I defined above is used for qualitative and comparison purposes only, accurate maps of the near-field and hot-spot topology being described in term of E/E_0 ratio.

To gain an insight into the topology of the hot spots generated by the NCs reported in this study, the total electric field to the incident electric field intensity ratio E/E_0 was plotted in a plane at 5 nm above the irradiated surface (figure 3). It is well known that when a noble-metal nanostructure is irradiated with an incident light beam, local enhancements of the scattered field may appear near the sharp edges, this finding acting almost as a principle in the design of SERS substrates [31, 32]. However, according to our calculation, depending on the geometry of the scatterer and the wavelength of the incident light, the hot spots may be localized at different positions. At 400 nm wavelength, the NCs characterized by a shape factor $d/2R$ of about 0.5, present localized hot spots either exactly onto the main symmetry axis (figure 3(a)) or near the tips (figures 3(a) and (b)) whether we use parallel or perpendicular polarized light, respectively. At this frequency the enhancement near the NC tips is small or comparable to that obtained near this median region. As the wavelength increases, a delocalization of the hot spots from the median region toward the NC tips occurs. This change is accompanied by significant increases in the hot-spot intensity (figures 3(c) and (d)). However, this increase is still dependent on the polarization of the light. The enhancement at 785 nm is greater than that at 400 nm for both parallel and perpendicular polarization states. Both localization and strength of the hot spots are dependent on the polarization state of the incident light, the difference between the parallel and the perpendicular modes being reversed in low and high frequency regimes: the hot spots are less intense in parallel polarized than in perpendicular polarized light at 400 nm (figures 3(a) and (b)) but it becomes slightly stronger in parallel polarized than in perpendicular polarized light at 785 nm (figures 3(c) and (d)). Thus, at 785 nm, the huge SERS enhancement obtained in our experiments can be mainly associated with the integrated hot spots from the tips of NC in both perpendicular and parallel polarized light.

To study the effect of the geometry of the NC on the SERS enhancement, we have fabricated several batches of NC samples with different openings and periods by using the EBL method. Typical SEM images observed at a tilting angle of 60° are shown in figure 4. In order to account for the effect of mutual interactions between neighbouring NCs in a given array, several samples consisting of Au and Ag arrays of NCs with identical external radii $R = 200$ nm and breadths $d = 150$ nm but different pitch sizes ranging from 500 nm up to 1000 nm were fabricated. Each sample consists of six dies populated with NCs with the same size and shape (thus having the same opening in design) but different pitch sizes and another six dies of NCs with the same size but different openings as obtained by changing the ratio of $d/2R$. The size of a die is about 80 μm by 80 μm whereas the distance between two neighbour dies is about 100 μm. All of the 12 different dies were fabricated onto the same Si substrate. The substrates were then coated with R6G molecules by the above mentioned method. It is assumed that the R6G molecules were uniformly distributed on each die in each sample. The quantity of interest in our analysis is the number of net counts (after the subtraction of the baseline) for the peak at 612 cm^{-1} as a function of the number of the NC per square micrometre. As shown in figure 5(a), the intensity of the Raman peak at 612 cm^{-1} increases with the number of NC per μm^2 although the data is a little bit scattered. This indicates that the output Raman signal measured in our system is a sum of contributions from each individual (non-interacting) NC. The far-field coupling [43–45] among adjacent NCs can be safely neglected with increasing the pitch size. Since the surface area of a single NC is about 5.5×10^{-8} mm^2 and the spot size of the laser is 25 μm, by extrapolating the linear dependence of the intensity for the 612 cm^{-1} peak versus the number of NCs, it is found that our Raman system is able to detect 100 NCs (with an objective 40× and 3 s of collecting time at power intensity of 0.15 mW μm^{-2}). As shown in the inset of figure 5(a), clear

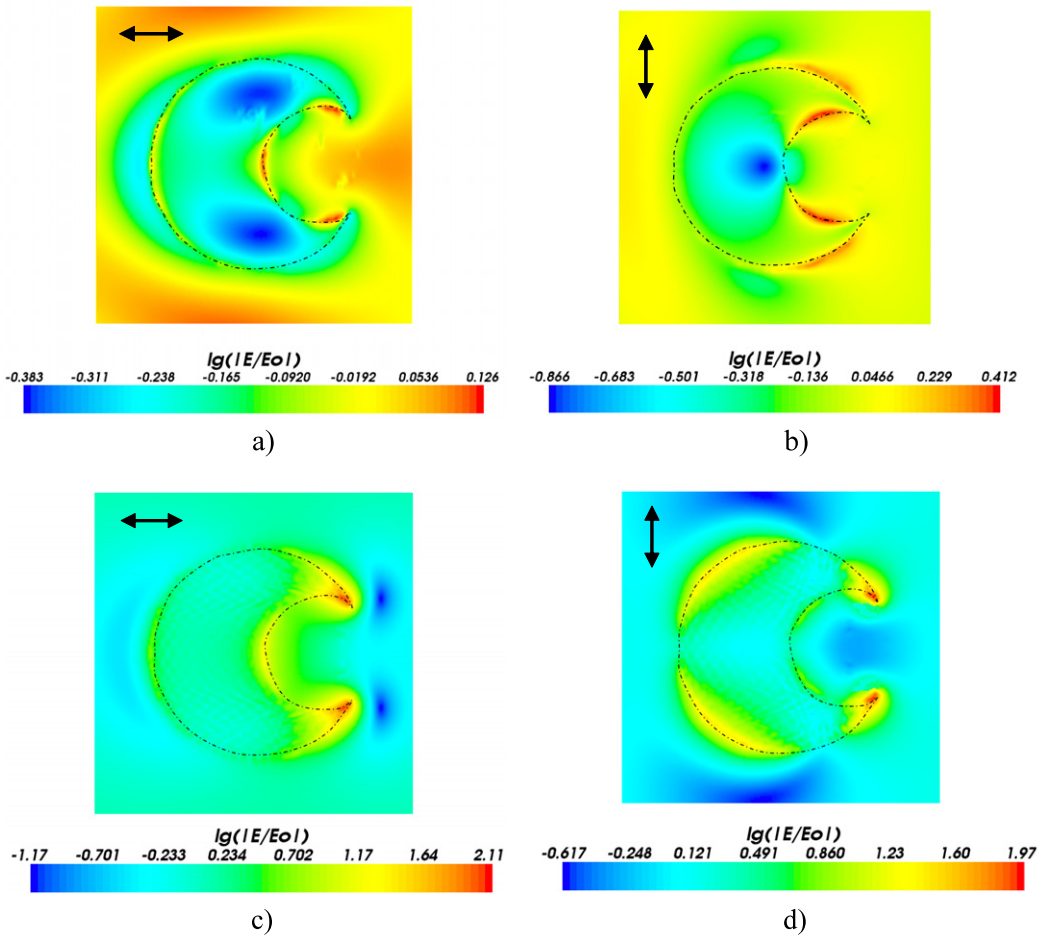

Figure 3. Scalar cut planes of $\lg(E/E_0)$ at 5 nm above a NC for two polarizations (as indicated with small arrows on each figure) and two wavelengths of the incident laser beam: (a) and (b), $\lambda = 400$ nm; (c) and (d), $\lambda = 785$ nm. The parallel and perpendicular polarization states are indicated by horizontal and vertical arrows, respectively.

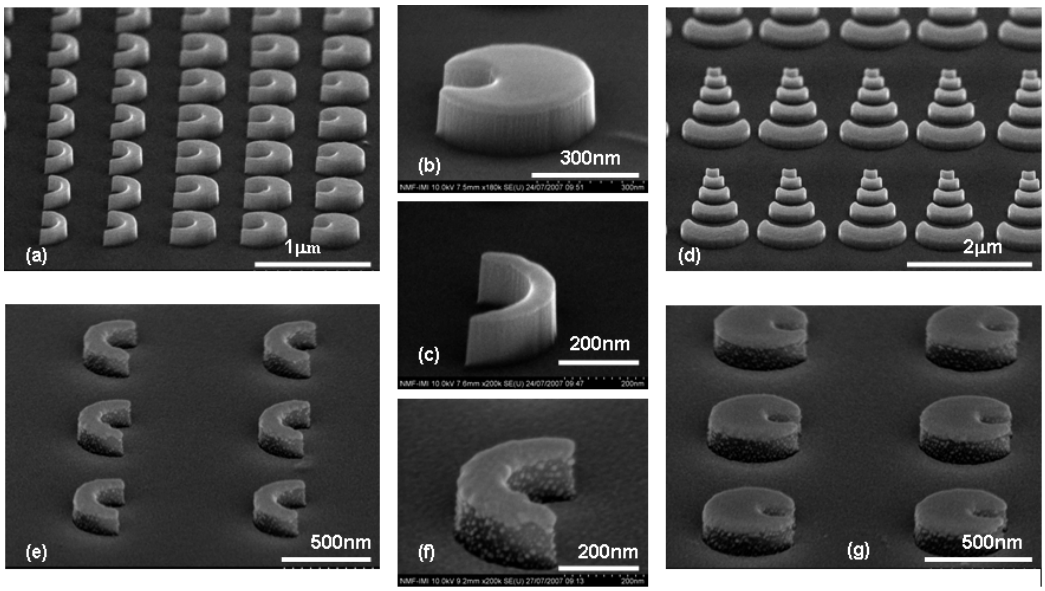

Figure 4. (a) SEM images of NCs with external curvature radius of $R = 200$ nm but different openings; (b) a NC with inner radius $r = 65$ nm; (c) a NC with inner radius $r = 170$ nm; (d) array of NCs with different external radii ranging from 400 nm down to 200 nm, immediately after RIE etching. (e)–(g) are images of the Au NCs after the deposition of 25 nm thick Au thin film on the top of the Si substrates.

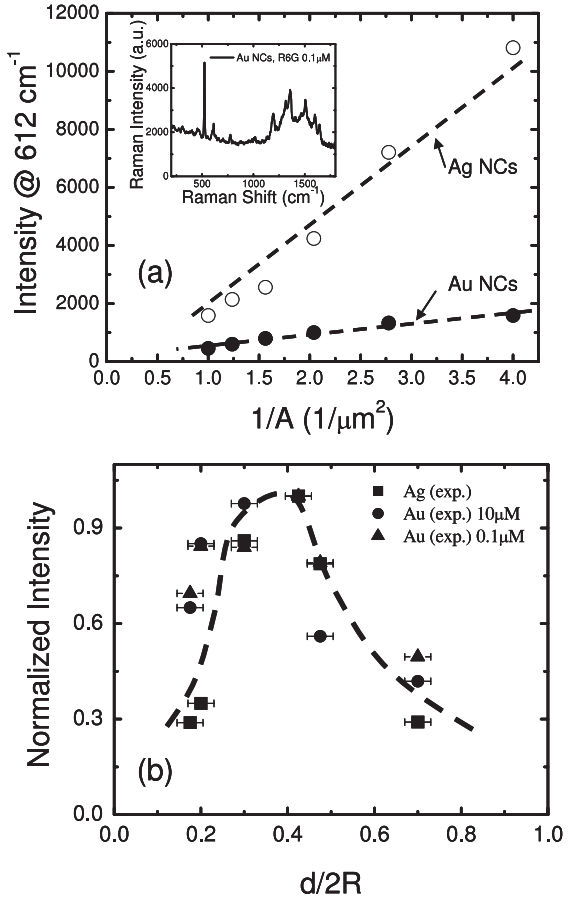

Figure 5. (a) Plot of the Raman intensity at 612 cm^{-1} as a function of $1/A$ for Au and Ag NCs. $1/A$ stands for the number of NCs per μm^2 whereas A is defined as the squared pitch size of the NC array. The inset of the figure shows the SERS spectrum acquired on Au NCs with an average thickness of 25 nm, $2R = 400$ nm and $d/2R = 0.25$. R6G molecules were coated at the concentration of 1×10^{-7} M. (b) Plot of the normalized counts of the SERS peak at 612 cm^{-1} versus the shape parameter $d/2R$ for 18 nm Ag NCs (squares), 25 nm Au NCs (discs) when the R6G molecules were coated at the concentration of 10 μM and Au NCs at the concentration of 0.1 μM (triangles). The dashed line is used for eye guidance only.

R6G SERS spectra have been obtained on the NCs substrate coated with R6G molecules at a concentration of 1×10^{-7} M. Similar to what was mentioned in [32], the enhancement factor of individual nanocrescent fabricated by our method is on the order of 10^{10} under the limitation of our Raman system. To make sure that the far-field coupling is minimized, a 1000 nm pitch size for the NC array is employed when we design the patterning of the nanocrescents with different openings.

Another quantity of interest in our analysis is the number of net counts for the peak at 612 cm^{-1} as a function of the shape parameter $d/2R$. Since we are interested in the influence of NC geometry on SERS, the intensity of the peak at 612 cm^{-1} for NCs with different values of $d/2R$ is measured. Figure 5(b) shows numerical values of the normalized intensity as function of $d/2R$. The maximum value of this intensity appears at the position of $d/2R = 0.4$, which corresponds to a breadth value of about 160 nm. The position of this peak

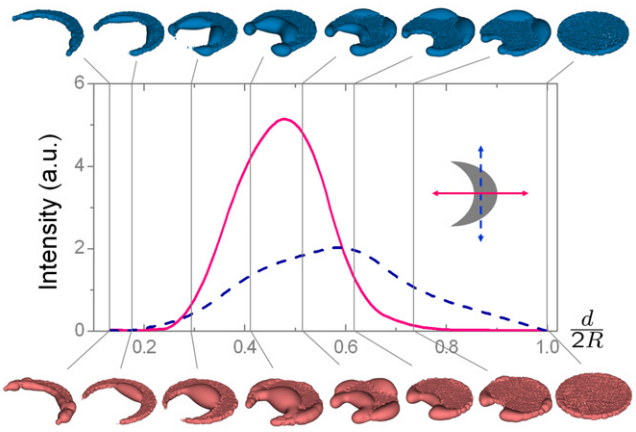

Figure 6. 3D representations of hot spots by drawing isosurfaces of constant $E/E_0 = 2.5$ in the near field at two polarizations of the incident laser beam ($\lambda = 785$ nm): parallel—bottom pictures and solid line in the graph—and perpendicular—top pictures/dashed line.

is almost independent of the nature of the noble metals when the thickness of Ag and Au is respectively 18 and 25 nm. In order to understand the underlying physical mechanisms, we have performed numerical computations of the near field for a series of NCs with constant $2R = 400$ nm but different values of shape parameter $d/2R$. Figure 6 shows the 3D representations of hot spots on these NCs obtained by drawing isosurfaces of constant $E/E_0 = 2.5$ in the near field at the two polarizations of the incident laser beam. For one of the extreme cases, for example, when $d/2R = 1$, the NC becomes a nanodisc, the hot spots are very weak if not absent all along the nanodisc contour in both polarization states and consequently the integration of the enhancement factor $(E/E_0)^4$ over the surface area of the nanodisc is very small even though this surface is the largest compared to the other NCs. When $d/2R$ is extremely small ($d/2R \sim 0.1$), some weak hot spots appear along the internal contour of the NC, the external contour (the longest one) being completely depleted of field enhancement, thus the integration of the enhancement factor is also very small under this condition. The maximum value of the SERS signal appearing at an intermediate value of the crescent shape parameter $d/2R$ may be explained as follows. For this geometry, both perpendicular and parallel modes present important values of the hot-spot intensity that complement each other well along the NC contour. However, the parallel configuration is much stronger (almost twice) than the perpendicular one, and it is assumed that the intensity of the Raman signal at optimal shape of the NC is dominated by the parallel mode. Around this aspect ratio, the perpendicular and parallel configurations of hot spots complement each other in a way that all NC contour is covered by regions of high enhancement of the electric field. Hot spots for all other geometries are either narrow and weak or restricted to certain limited regions of the NC contour. The small discrepancy in the peak position between the modelling (solid curve in figure 6) and experiment (dashed line in figure 5(b)) are probably due to the following two factors. Firstly, the morphology of

the fabricated NC is not perfect as the geometrical model used in the calculation. It is found that the tips of the NC become often rounded due to the technical limitation of the fabrication process. In addition, there are also variation in the size and geometry of the NCs even in the same die, as well as the fluctuation of the thickness of noble-metallic thin film, resulting in scattering of the experimental data point. Secondly, the theoretical computation is based on a single NC, but the experimental data were collected from a few hundred NCs covered by the laser spot used in the SERS measurement. All these effects are supposed also to be responsible for the wider peak in the experimental data compared to that obtained theoretically. Although the far-field intercoupling effects among NCs can be negligible, some interactions between the NC and the surrounding noble-metal film may also cause a shift in the SPR frequency and the distribution of the hot spots.

4. Conclusions

In summary, the SERS enhancement in detection of the R6G molecules has been studied on long-range ordered noble-metallic NCs which were successfully fabricated by both the NIL and EBL methods. The large SERS enhancement observed in NCs is attributed to the integrated hot spots presented on a stand alone noble NC. Both the geometry of the NCs and the wavelength of the excited laser can cause the redistribution of the hot spots on the NC surface; this results in the maximum of SERS intensity appearing at an intermediate value of the crescent eccentricity ($d/2R$ is in between 0.4 and 0.5) when a 785 nm laser is used as the excited light. Long-range ordered noble-metallic NCs with sharp tips and with size of about 160 nm and pitch size of 200 nm have been achieved by using a low-cost fabrication process based on the NIL method, which can lead to use of NCs as the SERS active substrate in practical applications.

Acknowledgments

This work was supported jointly by the Canada National Research Council (NRC) Genomics and Health Initiative Program, and by the NRC Industrial Materials Institute. We would like to thank the Réseau québécois de calcul de haute performance (RQCHP) for providing the computational resources.

References

[1] Fleischmann M, Hendra P J and McQuillan A J 1974 *Chem. Phys. Lett.* **26** 163
[2] Jeanmaire D J and Van Duyane R P 1977 *J. Electroanal. Chem.* **84** 1
[3] Kneipp K, Wang Y, Kneipp H, Perelman L T, Itzkan I, Dasari R R and Feld M S 1997 *Phys. Rev. Lett.* **78** 1667
[4] Nie S and Emory S R 1997 *Science* **275** 1102
[5] Baker G A and Moore D S 2005 *Anal. Bioanal. Chem.* **382** 1751
[6] Adrian J F 1982 *J. Chem. Phys.* **77** 5302
[7] Heller E, Sundberg R L and Tannor D 1982 *J. Phys. Chem.* **86** 1822
[8] Lombardi J R, Birke R L, Lu T and Xu J 1986 *J. Chem. Phys.* **84** 4174
[9] Persson B N J 1981 *Chem. Phys. Lett.* **82** 561
[10] Persson B N J, Zhao K and Zhang Z 2006 *Phys. Rev. Lett.* **96** 207401
[11] Moskovits M 2005 *J. Raman Spectrosc.* **36** 485
[12] Wang S, Pile D F P, Sun C and Zhang X 2007 *Nano Lett.* **7** 1076
[13] Anderson N, Bouhelier A and Novotny L 2006 *J. Opt. A: Pure Appl. Opt.* **8** S227
[14] Babadjanyan A J, Margaryan N L and Nerkararyan K V 2000 *J. Appl. Phys.* **87** 3785
[15] Stockman M I 2004 *Phys. Rev. Lett.* **93** 137404
[16] Bouhelier A, Renger J, Beversluis M R and Novotny L 2003 *J. Microsc.* **210** 220
[17] Mehtani D, Lee N, Hartschuh R D, Kisliuk A, Foster M D, Sokolov A P, Cajko F and Tsukerman I 2006 *J. Opt. A: Pure Appl. Opt.* **8** S183
[18] Nerkararyan K V, Abrahamyan T, Janunts E, Khachatryan R and Harutyunyan S 2006 *Phys. Lett.* A **350** 147
[19] Novotny L, Pohl D W and Hecht B 1995 *Ultramicroscopy* **61** 1
[20] Li K, Stockman M I and Bergman D J 2003 *Phys. Rev. Lett.* **91** 227402
[21] Liu Z, Steele J M, Srituravanich W, Pikus Y, Sun C and Zhang X 2005 *Nano Lett.* **5** 1726
[22] Gramotnev D K 2005 *J. Appl. Phys.* **98** 104302
[23] Gramotnev D K and Vernon K C 2007 *Appl. Phys.* B **86** 7
[24] Nerkararyan K V 1997 *Phys. Lett.* A **237** 103
[25] Pile D F P and Gramotnev D K 2006 *Appl. Phys. Lett.* **89** 041111
[26] Su K-H, Durant S, Steele J M, Xiong Y, Sun C and Zhang X 2006 *J. Phys. Chem.* B **110** 3964
[27] Jensen T R, Malinsky M D, Haynes C L and Van Duyne R P 2000 *J. Phys. Chem.* B **104** 10549
[28] Chen J *et al* 2005 *Nano Lett.* **5** 473
[29] Sherry L J, Chang S-H, Schatz G C, Van Duyne R P, Wiley B J and Xia Y 2005 *Nano Lett.* **5** 2034–8
[30] Wiley B J, Chen Y, McLellan J M, Xiong Y, Li Z-Y, Ginger D and Xia Y 2007 *Nano Lett.* **7** 1032–6
[31] Liu G L, Lu Y, Kim J, Doll J C and Lee L P 2005 *Adv. Mater.* **17** 2683
[32] Lu Y, Liu G L, Kim J, Mejia Y X and Lee L P 2005 *Nano Lett.* **5** 119–24
[33] Rochholz H, Bocchio N and Kreiter M 2007 *New J. Phys.* **9** 53
[34] Bukasov R and Shumaker-Parry J S 2007 *Nano Lett.* **7** 1113–8
[35] Cui B and Veres T 2007 *Microelectron. Eng.* **84** 1544
[36] Yurkin M A and Hoekstra A G 2007 *J. Quant. Spectrosc. Radiat. Transf.* **106** 558
[37] Yurkin M A, Maltsev V P and Hoekstra A G 2007 *J. Quant. Spectrosc. Radiat. Transf.* **106** 546
[38] Noguez C 2005 *Opt. Mater.* **27** 1204–11
[39] Druger S D and Bronk B V 1999 *J. Opt. Soc. Am.* B **16** 2239
[40] Brioude A, Jiang X C and Pileni M P 2005 *J. Phys. Chem.* **109** 13138
[41] Bosman M, Keast V J, Watanabe M, Maaroof A I and Cortie M B 2007 *Nanotechnology* **18** 165505
[42] Le Ru E C and Etchegoin P G http://arxiv.org/abs/physics/0504182
[43] Haynes C L, McFarland A D, Zhao L, Van Duyne R P, Gunnarsson L, Prikulis J, Kasemo B and Kall M 2003 *J. Chem. Phys.* B **107** 7337
[44] Lamprecht B, Schider G, Lechner R T, Ditbacher H, Krenn J R, Leitner A and Aussenegg F R 2000 *Phys. Rev. Lett.* **84** 4721
[45] Meier M, Wokaum A and Liao P F 1985 *J. Opt. Soc. Am.* B **2** 931